Electronic Supplementary Material (ESI) for Dalton Transactions.
This journal is © The Royal Society of Chemistry 2021

Two Tb-metal organic frameworks with different metal cluster nodes for C_2H_2/CO_2 separation

Lizhen Liu [a], Yaozong Chen [a], Zizhu Yao [b], Dinggui Chen [a], Quanjie Lin [b], Zhiwen Fan [b], Zhangjing Zhang [b], Binyi Chen [a,*] and Shengchang Xiang [b ,*]

[a] Key Laboratory of Polymer Materials and Products of Universities in Fujian, Department of Materials Science and Engineering, Fujian University of Technology, Fuzhou, Fujian 350108, China;

[b] Fujian Provincial Key Laboratory of Polymer Materials, College of Chemistry and Materials Science, Fujian Normal University, Fuzhou 350007, P. R. China.

E-mail: chenby@fjut.edu.cn; scxiang@fjnu.edu.cn.

Content

1. Experimental Section……S3

2. **Table S1** Crystal data and refinement results for the as-synthesized samples……... S7

3. **Fig. S1** The crystal structures and channel shapes in 2……S8

4. **Fig. S2** The PXRD patterns for 1 showing good agreement with simulated one for as-synthesized, solvent-exchanged by acetone…….……S9

5. **Fig. S3** The PXRD patterns for 1 in different temperature…….....S9

6. **Fig. S4** The PXRD patterns for 2 showing good agreement with simulated one for as-synthesized, solvent-exchanged by acetone……...S10

7. **Fig. S5** The PXRD patterns for 2 in different temperature……S10

8. **Fig. S6** TGA curve of 1 and 2……S11

9. **Fig. S7** The pore size distribution of 1a and 2a……S12

10. **Fig. S8** Single-component adsorption isotherms of 1a at 273 K……S12

11. **Fig.S9** The plots of virial equation of C_2H_2 in 1a…….……..S13

12. **Fig. S10** The plots of virial equation of CO_2 in 1a……S13

13. **Fig. S11** C_2H_2 and CO_2 adsorption enthalpy curves on 1a……S14

14. **Fig. S12** Single-component adsorption isotherms of 2a at 273 K……..S14

15. **Fig. S13** The plots of virial equation of C_2H_2 in 2a……S15

16. **Fig. S14** The plots of virial equation of CO_2 in 2a……S15

17. **Fig. S15** C_2H_2 and CO_2 adsorption enthalpy curves on 2a…….…S16

18. **Fig. S16** Schematic illustration of the breakthrough experimental setup…….…….S16

19.**Fig. S17** view of ellipsoid graph showing the asymmetric unit (a) and 3D structure (b) of compound 1……..S17

20. **Fig. S18** view of ellipsoid graph showing the asymmetric unit (a) and 3D structure (b) of compound 2……...S17

21. **Table S2** Solvent masks information for 1 and 2……S17

22. **References**……..S17

Experimental Section

Materials and Methods

All reagents and solvents used in synthetic studies are commercially available and were used as supplied without further purification. 2-fluorobenzoic acid (2-FBA) and metal salt were purchased from Tansoole. Powder X-ray diffraction (PXRD) was carried out with a PANalytical X'Pert[3] powder diffractometer equipped with a Cu sealed tube (λ = 1.541874 Å) at 40 kV and 40 mA over the 2θ range of 5-30°. The simulated pattern was produced using the Mercury V1.4 program and single-crystal diffraction data. Thermal analysis was carried out on a METTLER TGA/SDTA 851 thermal analyzer from 30 to 600 ^{o}C at a heating rate of 10 ^{o}C min^{-1} under N_2 flow. Elemental analyses (C, H and N) were performed on a Perkin-Elmer 240C analyzer.

Single-crystal X-ray structural analysis

Data collection and structural analysis of **1** and **2** were performed on an Agilent Technologies SuperNova single crystal diffractometer equipped with graphite monochromatic Mo Ka radiation (λ = 0.71073 Å). The crystal was kept at 293 K during data collection. Using Olex2[1], the structure was solved with the Superflip[2] structure solution program using charge flipping and refined with the ShelXL[3] refinement package using least squares minimization. All nonhydrogen atoms were refined with anisotropic displacement parameters. The hydrogen atoms on the ligands were placed at idealized positions and refined using a riding model. We employed PLATON[4] and SQUEEZE[5] to calculate the diffraction contribution of the solvent molecules and thereby produce a set of solvent-free diffraction intensities. The detailed crystallographic data and structure refinement parameters for these compounds are summarized in Table S1 (CCDC: 2056375-2056376).

Gas Sorption Measurements

After the bulk of the solvent was decanted, the freshly prepared sample of **1** and **2** (~0.15 g) was soaked in ~10 mL of acetone for 1 h, and then the solvent was decanted, respectively. Following the procedure of acetone soaking and decanting 20 times, the solvent-exchanged samples were activated by vacuum at 80 ^{o}C overnight until a pressure of 5 μmHg to obtain the activated **1a** and **2a**, respectively. N_2, CO_2, C_2H_2 adsorption isotherms were measured on Micromeritics ASAP 2020 HD88 surface area analyzer for the activated **1a** and **2a**. As the center-controlled air condition was set up at 23 ^{o}C, a water bath of 23 ^{o}C was used for adsorption isotherms at 296 K, whereas liquid nitrogen and ice-water baths were used for the isotherms at 77 K and 273 K, respectively.

Adsorption Enthalpy Calculation. The C_2H_2 and CO_2 adsorption enthalpy (Q_{st}) of the activated **1a** and **2a** was calculated using adsorption data at 273 K and 296 K. A virial-type expression (eq S1) was used to fit these data, and then the Q_{st} was then calculated by the expression given by eq S2.

$$InP = In(n) + \frac{1}{T}\sum_{i=0}^{m} a_i n^i + \sum_{i=0}^{n} b_i n^i \quad \text{(S1)}$$

$$Q_{st} = -R\sum_{i=0}^{m} a_i n^i \quad \text{(S2)}$$

Here, P, n, and T are the pressure, amount adsorbed, and temperature, respectively. m and n determine the number of terms required to adequately describe the isotherm. a_i and b_i are virial coefficients.

Prediction of the Gas Adsorption Selectivity by IAST: The C_2H_2/CO_2 selectivity of the activated **1a** and **2a** were estimated by ideal adsorbed solution theory (IAST) theory. In this work, the measured experimental data is excess loadings (q^{ex}) of the pure components CO_2 and C_2H_2 for the activated **1a** and **2a**, which should be converted to absolute loadings (q) firstly.

$$\mathrm{q} = q^{ex} + \frac{pV_{pore}}{ZRT}$$

Here Z is the compressibility factor. The Peng-Robinson equation was used to estimate the

value of compressibility factor to obtain the absolute loading, while the measure pore volume of **1a** and **2a** is 0.54 cm^3/g and 0.26 cm^3/g, respectively.

The single-site Langmuir-Freundlich equation is used for fitting the isotherm data at 296 K and 273 K, respectively.

$$q = q^{\max} \frac{bp^{1/n}}{1 + bp^{1/n}}$$

Here p is the pressure of the bulk gas at equilibrium with the adsorbed phase (kPa), q is the adsorbed amount per mass of adsorbent (mmol/g), q^{max} is the saturation capacities of site 1 (cm^3/g), b is the affinity coefficients of site 1 (1/kPa), n is the deviations from an ideal homogeneous surface.

The adsorption selectivity for C_2H_2/CO_2 separation is defined by

$$S = \frac{q_1/q_2}{p_1/p_2}$$

q_1 and q_2 are the molar loadings in the adsorbed phase in equilibrium with the bulk gas phase with partial pressures p_1, and p_2. We calculate the values of q_1 and q_2 using the Ideal Adsorbed Solution Theory (IAST) of Myers and Prausnitz[6].

Dynamic Gas Breakthrough Experiments

The mixed-gas breakthrough separation experiment was conducted at 296 K using a lab scale fix-bed reactor [7]. In a typical experiment, **1a** and **2a** (~1.6 g) were packed into a quartz tube column (the quartz tube column was 45 cm in length with a 5 mm inner diameter) with silica wool filling the void space, respectively. The sorbent was activated *in-situ* in the column with a vacuum pump at 353 K for overnight. A helium flow (10 mL/min) was used after the activation process to purge the adsorbent. The flow of He was then turned off, while a gas mixture of 5% C_2H_2, 5% CO_2 and 90% He at 4 mL/min was allowed to flow into the column. The outlet composition was continuously monitored by gas chromatograph until complete breakthrough was achieved. On the basis of the gas balance, the gas adsorption capacities can be determined as follows [8,9]:

$$q_i = \frac{C_i V}{22.4 \times m} \times \int_0^t (1 - \frac{F}{F_0}) dt$$

Where q_i is the equilibrium adsorption capacity of gas i (mmol/g), C_i is the feed gas concentration, V is the volumetric feed flow rate (cm^3/min), t is the adsorption time (min), F_0 and F are the inlet and outlet gas molar flow rates, respectively, and m is the mass of the adsorbent (g). The separation factor (α) of the breakthrough experiment is determined as:

$$\alpha = \frac{q_1 y_2}{q_2 y_1}$$

In which y_i is the molar fraction of gas i in the gas mixture.

Synthesis

Synthesis of pyridine-2,4,6-tribenzoic acid (H_3PTB)

It was synthesized according to the literature [10,11].

Synthesis of 1: $((CH_3)_2(NH_2))_2[Tb_9(\mu_3\text{-}OH)_8(\mu_2\text{-}OH)_3(PTB)_6]\cdot(DMF)_{14}\cdot(H_2O)_{19}$. A mixture of H_3PTB (0.044 g, 0.1 mmol), $Tb(NO_3)_3$ (0.045 g, 0.1 mmol), 2-FBA (0.14 g, 1 mmol) were dissolved in DMF (3 mL) and H_2O (0.2 ml) by ultrasound and then added HNO_3 (0.3 ml, 3.5 M). Ultimately, the resulting yellow solution was sealed in vessel (20 mL), which was heated in 100 ^oC for 5 day. After cooling to ambient temperature, yellow block crystals were obtained, washed by DMF and dried in air.

Elemental analysis calcd (%) for **1**, $C_{202}H_{247}N_{22}O_{80}Tb_9$: C 42.61, H 4.37, N 5.41; found: C 40.67, H 4.53, N 5.56.

Synthesis of 2: $[(CH_3)_2NH_2]_3\{[Tb_9(\mu_3\text{-}O)_2(\mu_3\text{-}OH)_{12}(H_2O)_6][Tb_3(\mu_3\text{-}O)(HCO_2)_3(PTB)_6]\}\cdot(DMF)_{12}\cdot(H_2O)_7$. A mixture of H_3PTB (0.044 g, 0.1 mmol), $Tb(NO_3)_3$ (0.045 g, 0.1 mmol), 2-FBA (0.14 g, 1 mmol) were dissolved in DMF (6 mL) and H_2O (0.5 ml) by ultrasound and then added HNO_3 (0.3 ml, 3.5 M). Ultimately, the resulting yellow solution was sealed in Teflon-lined autoclave (20 mL), which was heated in 120 ^oC for 3 day. After cooling to ambient temperature, yellow flake crystals were obtained, washed by DMF and dried in air.

Elemental analysis calcd (%) for **2**, $C_{201}H_{233}O_{82}N_{21}Tb_{12}$: C 39.18, H 3.81, N 4.77; found: C 39.77, H 3.92, N 4.96.

Table S1 Crystal data and refinement results for the as-synthesized samples.

Identification code	**1**	**2**
CCDC	2056375	2056376
Empirical formula	$C_{202}H_{247}N_{22}O_{80}Tb_9$	$C_{201}H_{233}O_{82}N_{21}Tb_{12}$
Formula weight	5693.55	6162.20
Temperature/K	293(2)	293(2)
Crystal system	hexagonal	hexagonal
Space group	*P6₃/mmc*	*P6₃/mmc*
a/Å	22.4708(2)	22.2999(3)
b/Å	22.4708(2)	22.2999(3)
c/Å	32.9771(5)	29.1681(7)
α/°	90	90
β/°	90	90
γ/°	120	120
V/Å^3	14420.5(3)	12561.6(5)
Z	2	2
ρ_{calc}g/cm^3	0.973	1.342
μ/mm^{-1}	2.220	3.391
F(000)	4046.0	4812.0
Radiation	MoKα (λ = 0.710)	MoKα (λ = 0.710)
Data/restraints/parameters	4614/148/183	4658/19/210
Goodness-of-fit on F^2	1.037	1.098
Final R indexes [I>=2σ (I)][a]	R_1 = 0.0995,	R_1 = 0.0841,
	wR_2 = 0.2580	wR_2 = 0.2387
Final R indexes [all data][a]	R_1 = 0.1078,	R_1 = 0.1022,
	wR_2 = 0.2666	wR_2 = 0.2548

[a]$R_1 = \sum(|F_o| - |F_c|) / \sum|F_o|$, [b]$wR_2 = [\sum w(F_o^2 - F_c^2)^2 / \sum w(F_o^2)^2]^{0.5}$

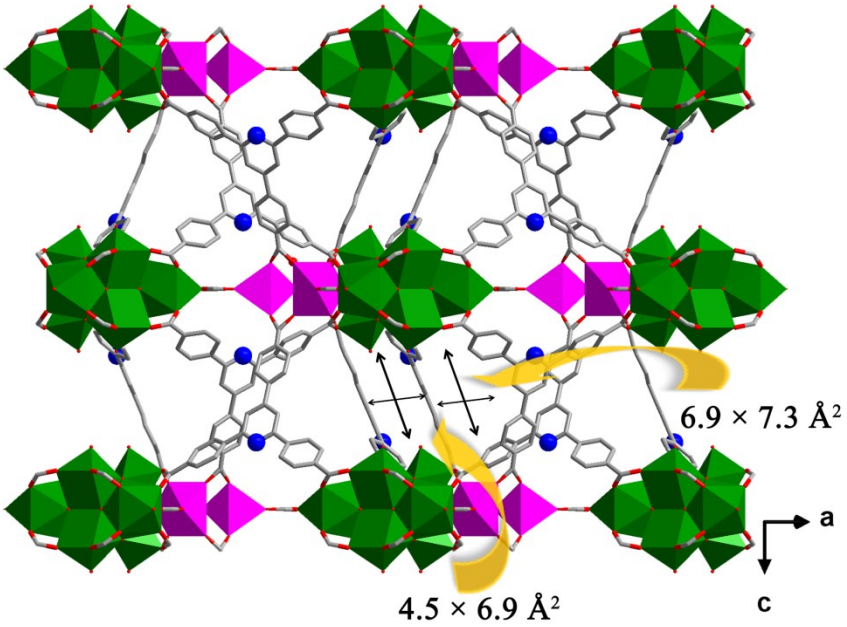

Fig. S1. The crystal structures and channel shapes in **2.**

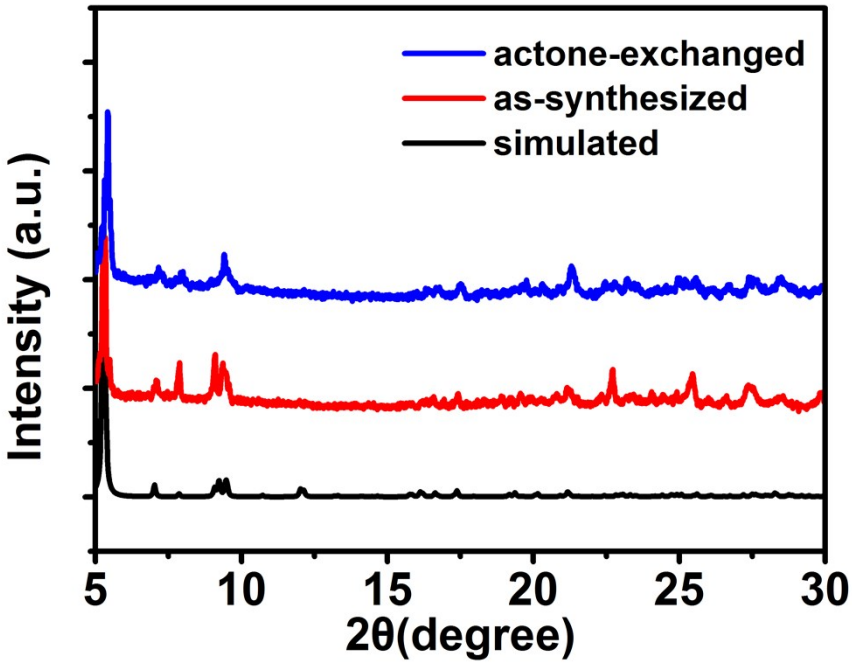

Fig. S2. The PXRD patterns for **1** showing good agreement with simulated one for as-synthesized, solvent-exchanged by acetone.

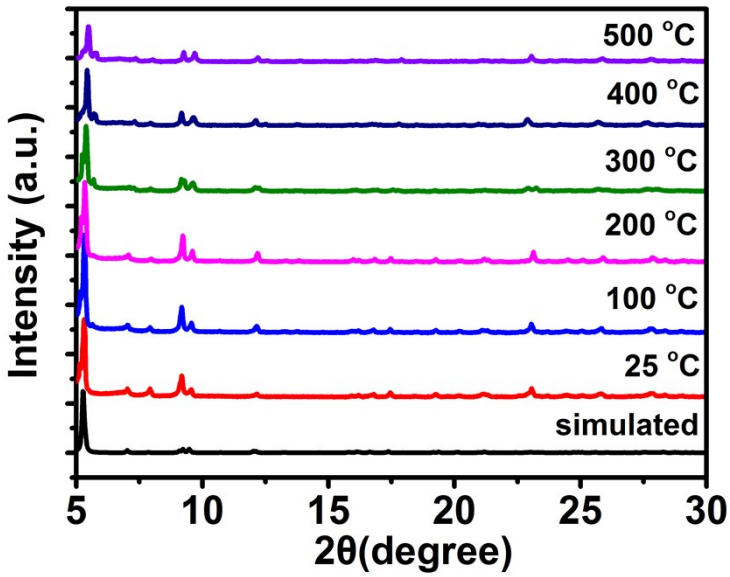

Fig. S3. The PXRD patterns for **1** in different temperature.

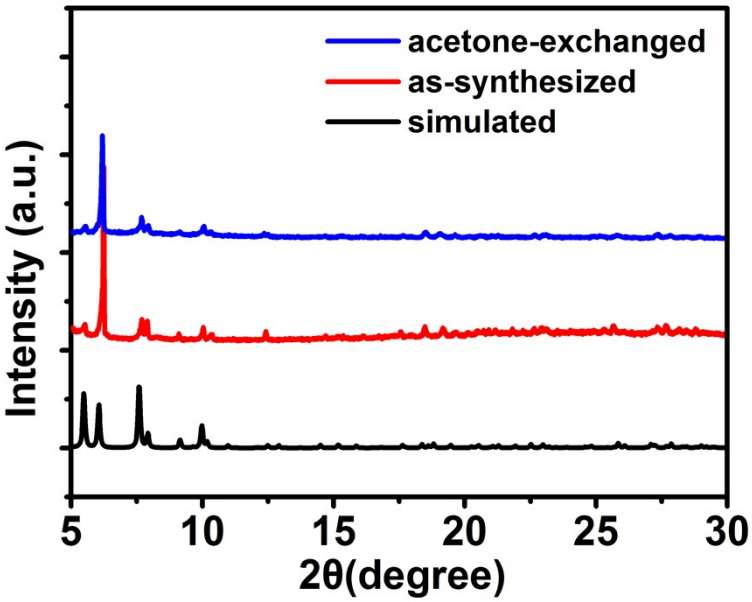

Fig. S4. The PXRD patterns for **2** showing good agreement with simulated one for as-synthesized, solvent-exchanged by acetone.

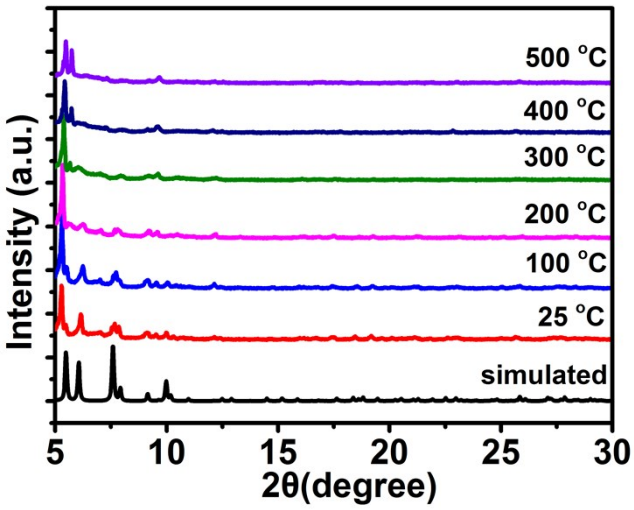

Fig.S5. The PXRD patterns for **2** in different temperature

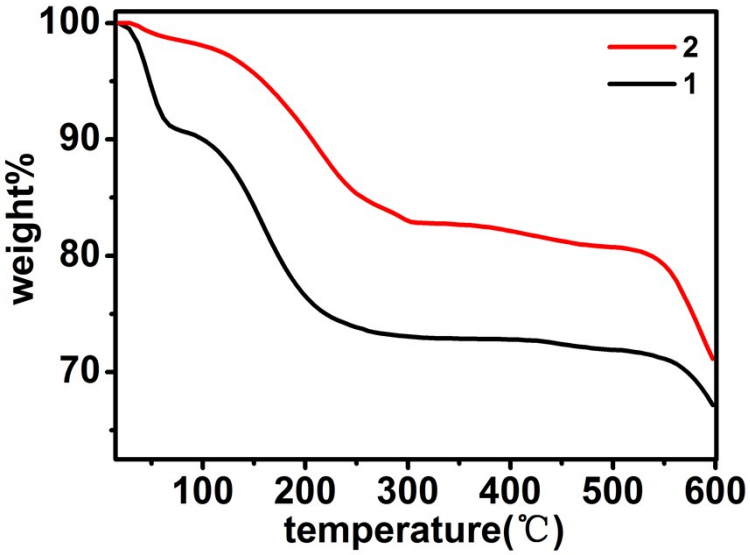

Fig. S6. TGA curve of **1** and **2**.

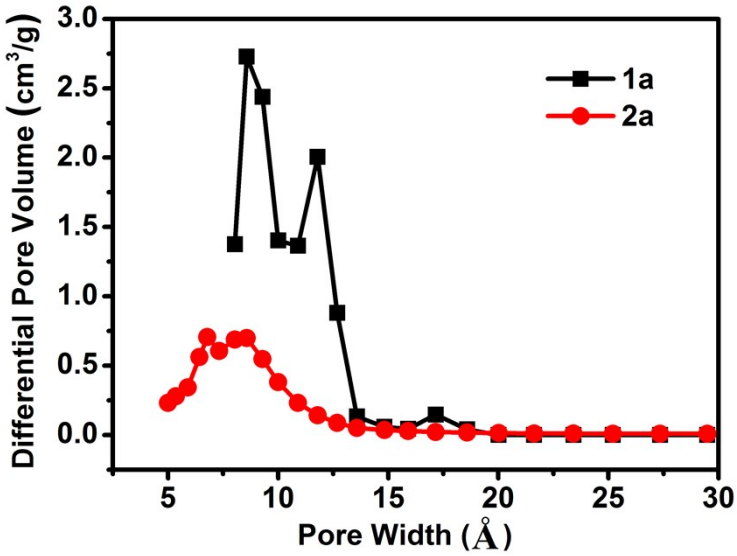

Fig. S7. The pore size distribution of **1a** and **2a**.

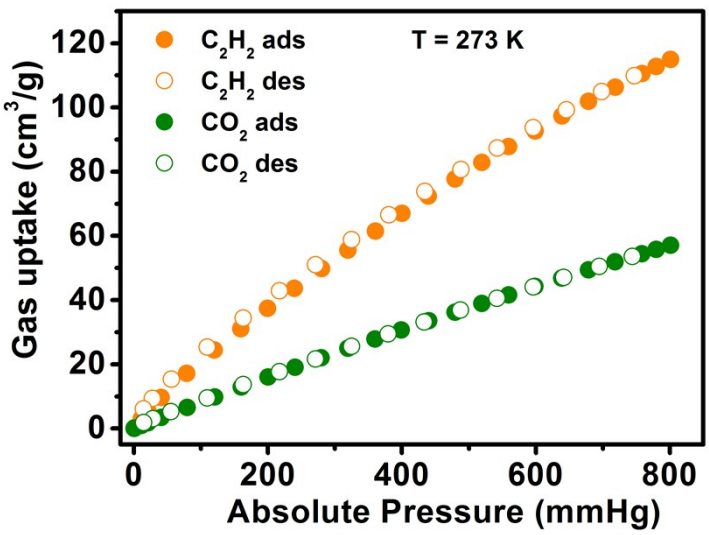

Fig. S8. Single-component adsorption isotherms of **1a** at 273 K.

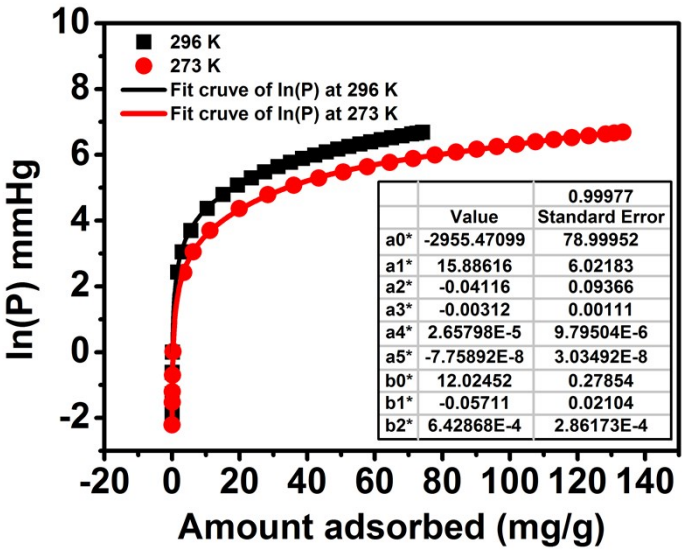

Fig. S9. The plots of virial equation of C_2H_2 in **1a**.

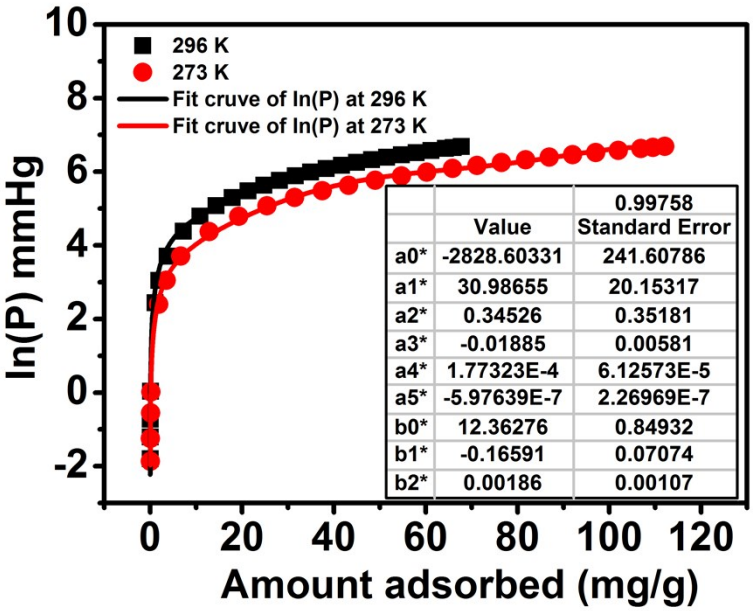

Fig. S10. The plots of virial equation of CO_2 in **1a**.

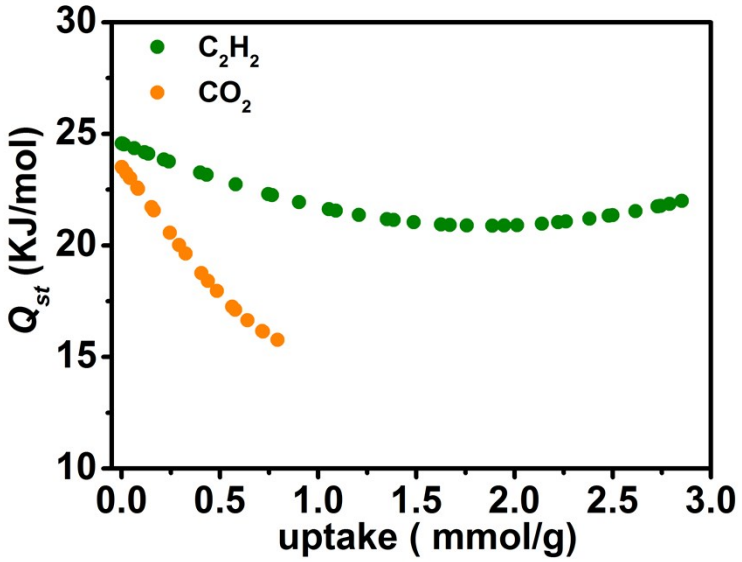

Fig. S11. C_2H_2 and CO_2 adsorption enthalpy curves on **1a**.

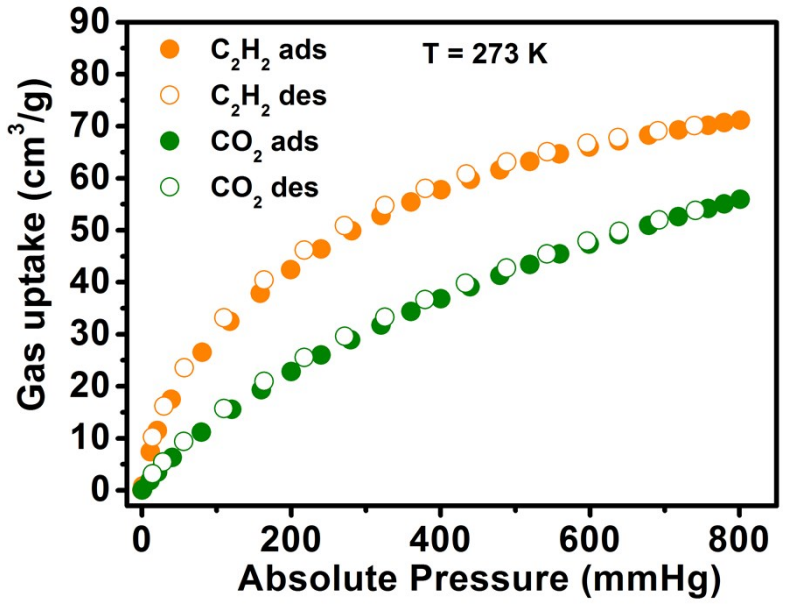

Fig. S12. Single-component adsorption isotherms of **2a** at 273 K.

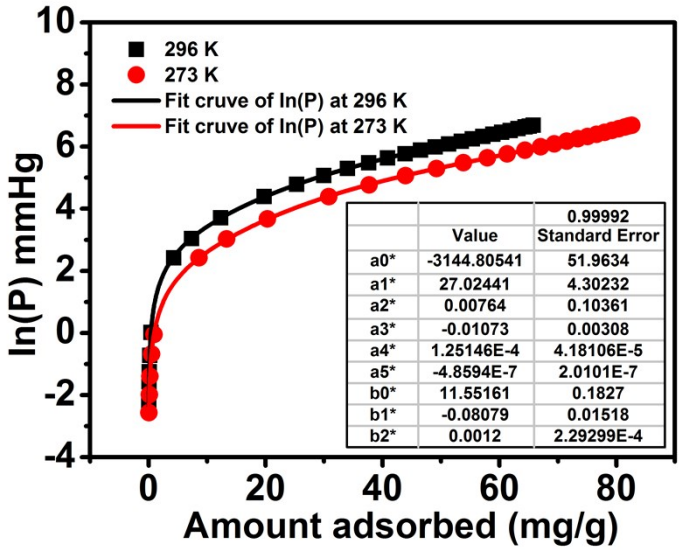

Fig. S13. The plots of virial equation of C_2H_2 in **2a**.

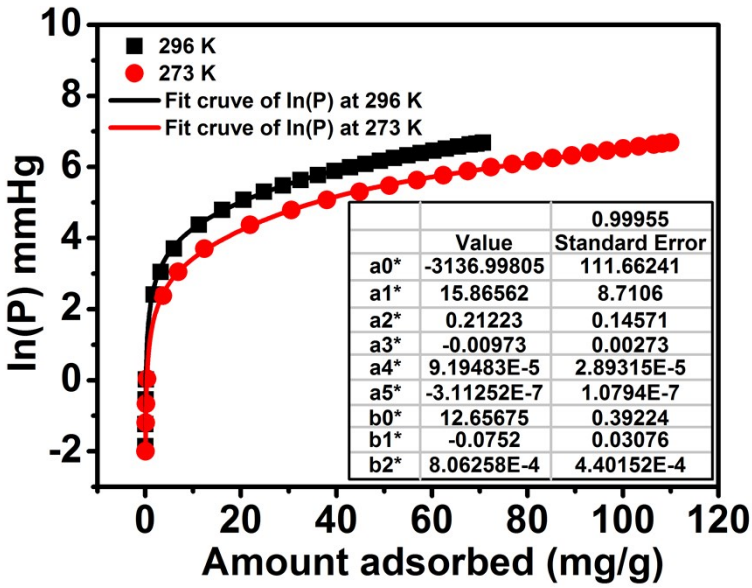

Fig. S14. The plots of virial equation of CO_2 in **2a**.

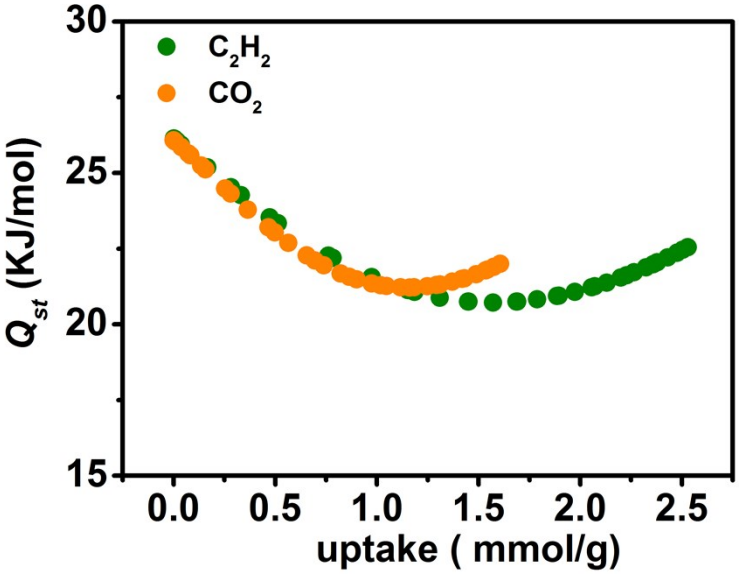

Fig. S15. C_2H_2 and CO_2 adsorption enthalpy curves on **2a**.

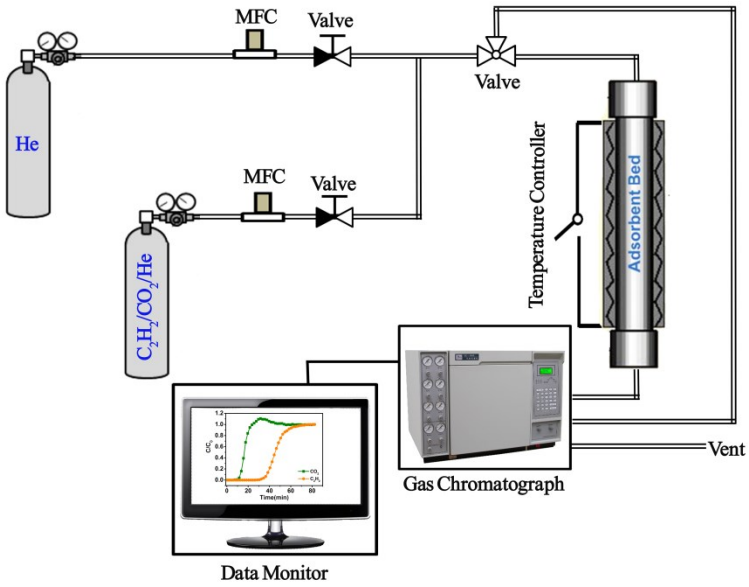

Fig. S16. Schematic illustration of the breakthrough experimental setup.

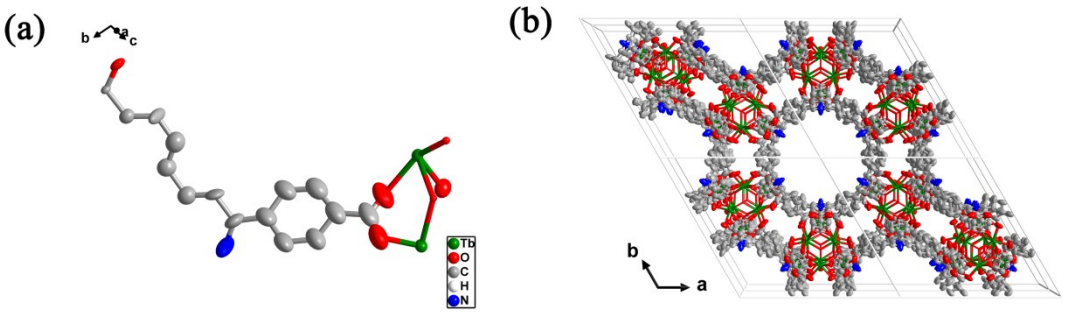

Fig. S17 view of ellipsoid graph showing the asymmetric unit (a) and 3D structure (b) of compound **1**.

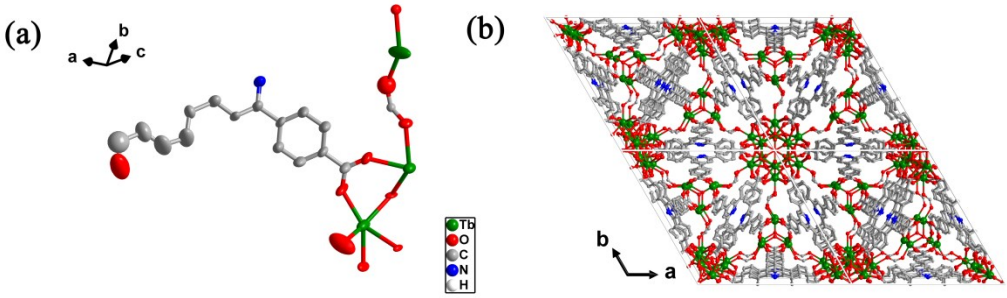

Fig. S18 view of ellipsoid graph showing the asymmetric unit (a) and 3D structure (b) of compound **2**.

Table S2 Solvent masks information for **1** and **2**.

Compound	Number	X	y	z	Volume	Electron count	Content
1	1	-0.569	-0.778	-0.817	9050.3	2285.8	DMF,H_2O,$[(CH_3)_2NH_2]^+$
2	1	-0.154	-0.141	0.006	6095	1680	DMF,H_2O,$[(CH_3)_2NH_2]^+$

References

(1) A. V. Dolomanov, L. J. Bourhis, R. J. Gildea, et al., *J. Appl. Crystallogr*. 2009, **42**, 339–341.
(2) L. Palatinus, G. Chapuis, *J. Appl. Crystallogr*. 2007,**40**, 786-790.
(3) G. M. Sheldrick, Acta Crystallogr., *Sect. A: Found. Crystallogr*. 2008,**64** ,112-122.
(4) L. Sarkisov, A. Harrison, *Mol. Simul*., 2011, **37**, 1248-1257.
(5) A. L. Spek, *J. Appl. Crystallogr*. 2003,**36**,7-13.
(6) A. L. Myers, J. M. Prausnitz, *AIChE J*, 1965,**11**,121-127.
(7) L. Z. Liu, Z. Z. Yao, Y. X. Ye, et al., *Inorg. Chem*. 2018, **57**, 12961-12968.
(8) H. Chang, Z. X. Wu, *Ind. Eng. Chem. Res*. 2009,48,4466-4473.
(9) J. Liu, J. Tian, P. K. Thallapally, B. P. McGrail, *J. Phys.Chem. C* 2012,116 ,9575-9581.
(10) J. X. Yang, X. T. Tao, C. X. Yuan, et al., *J. Am. Chem. Soc*. 2005,127,3278-3279.

(11) Q. Yao, A. B. Gómez, J. Su, et al., *Chem. Mater*. 2015,**27**,5332-5339.